EXTENSIONAL FLOW OF ERYTHROCYTE MEMBRANE FROM CELL BODY TO ELASTIC TETHER

II. Experiment

R. M. HOCHMUTH, H. C. WILES, E. A. EVANS, AND J. T. MCCOWN
Department of Biomedical Engineering, Duke University, Durham, North Carolina 27706

ABSTRACT This is the second of two papers on an analytical and experimental study of the flow of erythrocyte membrane. In the experiments discussed here, preswollen human erythrocytes are sphered by aspirating a portion of the cell membrane into a small micropipette; and long, thin, membrane filaments or tethers are steadily withdrawn from the cell at a point diametrically opposite to the point of aspiration. The aspirated portion of the membrane furnishes a reservoir of material that replaces the membrane as it flows as a liquid from the nearly spherical cell body to the cylindrical tether. The application of the principle of conservation of mass permits the tether radius R_t to be measured with the light microscope as the tether is formed and extended at a constant rate. The tether behaves as an elastic solid such that the tether radius decreases as the force or axial tension acting on the tether is increased. For the range of values for R_t in these experiments (100 Å $\leq R_t \leq$ 200 Å), the slope of the tether-force, tether-radius line is -1.32 dyn/cm. The surface viscosity of the membrane as it flows from cell body to tether is 3×10^{-3} dyn·s/cm. This viscosity is essentially constant for characteristic rates of deformation between 10 and 200 s^{-1}.

INTRODUCTION

As illustrated in Fig. 1, we have created an experiment in which the erythrocyte membrane can flow continuously off (or on) the spherically shaped body of an erythrocyte. As membrane material leaves the cell it forms a cylindrically shaped "tether" which stretches between the cell body and a small latex bead. Moving the bead at a constant rate creates an axial tension in the elastic tether that differs from the isotropic tension in the membrane. A positive tension difference (when the axial tension in the tether exceeds the isotropic tension in the membrane) is caused by the extensional flow of membrane material onto the tether as the bead is moved away from the cell body, whereas a negative tension difference is caused by the reverse process. When we use the equations of membrane mechanics and fluid mechanics to analyze this process (Hochmuth and Evans, 1982), we find the tether radius must decrease as the velocity of the tether is increased in a positive direction (i.e., away from the cell) and this decrease depends on the viscosity of the membrane and the elasticity of the tether. Both the membrane viscosity and the tether elasticity can be measured by performing a series of experiments at different velocities and different isotropic tensions in the membrane.

In classic experiments in fluid mechanics, such as Hagen-Poiseuille flow through a tube or Couette flow between counter-rotating cylinders, the liquid material is contained in a geometrically simple system. Flow in the system is created by the application of stresses at the boundary of the material. Analysis and measurement of the stress-flow behavior of the liquid leads to the characterization and measurement of its viscosity. This approach is at work in the present study. In our case, tensions are applied at the boundaries (the tether and the cell body) and flow is created in a well-defined, axisymmetric disklike region around the tether. The flow is readily manipulated; that is, it can be reversed or it can continue in the positive direction until all of the material in the reservoir (the pipette) is exhausted. Thus, these experiments are in the tradition of the original viscous flow experiments in fluid mechanics, although here we are dealing with a viscous material which is only a few molecules thick.

MATERIALS AND METHODS

A 1–2 μl drop of fresh human blood is obtained from a finger prick immediately before an experiment. The drop is diluted with 10 ml of filtered phosphate-buffered saline (3.55 g/liter NaCl, 3.38 g/liter $Na_2HPO_4 \cdot 7H_2O$, and 0.327 g/liter KH_2PO_4, pH = 7.4) with an osmolarity of 150 mosM as measured with a freezing-point depression osmometer. This relatively low osmolarity will swell the cells to a nearly spherical shape. Albumin in small concentration (0.05 to 0.083 g/100 ml) is added to the solution to prevent cell crenation. In addition, small concentrations of 2–3 μm diameter latex beads (Dow Corning Corp., Midland, MI.) are added to the suspension, and the beads and cells are allowed to adhere to

Dr. Evans' present address is the Department of Pathology, University of British Columbia, Vancouver, B. C., Canada V6T 1W5; and Dr. McCown's present address is the Lever Brothers Research Center, Edgewater, New Jersey 07020.

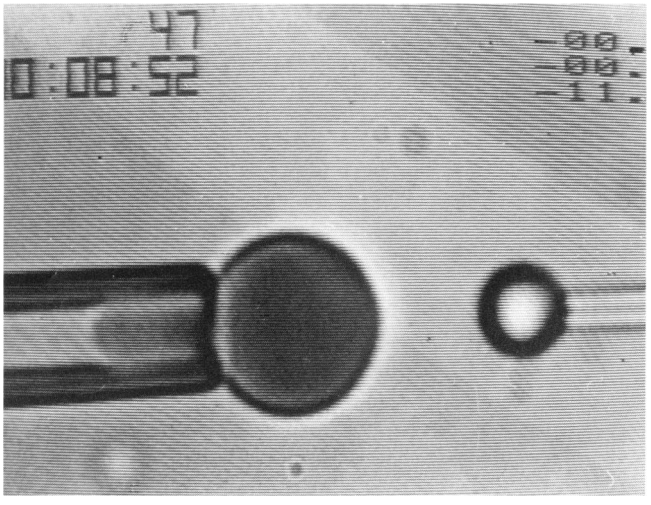

FIGURE 1 Preswollen red cell aspirated into a 2-μm diameter pipette. A long, thin membrane filament or tether stretches between the spherical erythrocyte and the small latex bead which is held with a second pipette.

each other to form, in some instances, "cell-bead pairs." In a few instances, sphered and glutaraldehyde-fixed erythrocytes are used instead of the latex beads. In addition, to promote adhesion between membrane and latex bead, the beads are presoaked in a dilute concentration (40 μg/ml) of wheat germ agglutinin.

The solution of cells and beads is injected into a microchamber (1 cm $\times$ 1.5 cm $\times$ 0.1 cm) open on two opposite sides. This allows the insertion of a micropipette into each side of the chamber as shown in Figs. 1 and 2. The chamber is mounted on a Leitz Diavert microscope (Fig. 2; E. Leitz Inc., Rockleigh, NJ) equipped with 25$\times$ eyepieces and a 40$\times$, 0.65 NA long working-distance Nikon objective (Nikon Inc., Garden City, NJ). The field is illuminated with monochromatic light (4,363 Å) from an Oriel 200-W Hg vapor lamp (Oriel Corp. of America, Stamford, CT), narrow band-pass interference filter and 0.70 NA long working-distance condensor. The image from a high resolution video camera (Dage-MTI, Michigan City, IN) with 75-mm lens is recorded with a 3/4-inch video cassette recorder (Sony VO-2800) and displayed on a 17-inch monitor (Setchel-Carlson Electronics, Inc., New Brighton, MN).

A pneumatically-controlled micromanipulator (DeFonbrune) mounted directly on the microscope stage (Fig. 2) is used to manipulate a micropipette with a 2.0 μm (i.d.) tip. (Note that the micropipette mounted in the micromanipulator shown on the right-hand side of the microscope in Fig. 2 is shown on the left-hand side of Fig. 1 because of a reversal of the image by the microscope). The micropipette is filled (by boiling in a partial vacuum) with the same phosphate-buffered saline

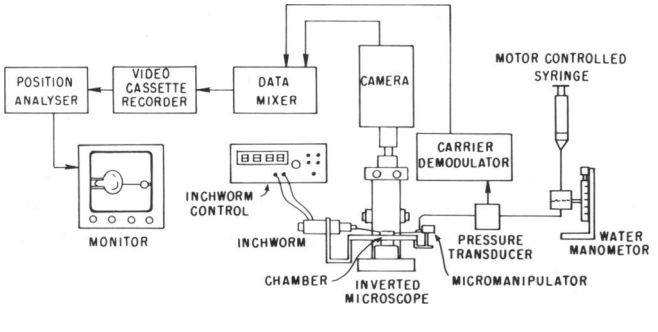

FIGURE 2 Diagram of experimental system. The Inchworm shown on the left-hand side of the microscope holds the small pipette shown on the right-hand side of Fig. 1.

solution in which the cells are suspended. The pressure in the pipette is "nulled" with a water manometer which is attached to the micropipette with a water-filled plastic tube (Fig. 2). (The null point occurs when a cell at the mouth of the pipette moves neither towards nor away from the pipette). An aspiration pressure is produced by withdrawing a motor-controlled syringe which is "air-coupled" to the manometer reservoir (Fig. 2). The pressure in the pipette is measured with a pressure transducer (Validyne Engineering Corp., Northridge, CA) and displayed on the video screen by a "data mixer" (Vista Electronics, La Mesa, CA.). The data mixer also provides the time, including a 1/60 s frame counter, directly on the video screen.

An electromechanical linear translator or "Inchworm" (Burleigh Instruments Inc., Fishers, NY) is mounted on the left-hand side of the microscope stage and holds a second smaller pipette (shown as the right-hand pipette in Fig. 1). The linear translator moves the smaller pipette either into or out of the chamber at a controlled and constant rate. This system has a digital display that indicates the linear displacement of the pipette.

In an experiment, a cell-bead pair is identified and the cell is aspirated into the pipette at a point opposite to the point where the bead is attached (Fig. 1). A strong aspiration pressure holds the bead in the second, smaller pipette and the bead is slowly withdrawn by the linear translator while the erythrocyte aspiration pressure is held constant. An invisible tether is stretched between the cell body and bead (Fig. 1) and as the tether is increased in length, the aspirated portion of the membrane decreases in length. The return of the bead causes the aspirated portion of the membrane to return essentially to its initial location. The displacement of the membrane within the pipette is measured with a position analyzer (Vista Electronics) which imposes two movable cursors on the video screen and provides a digital reading which is proportional to the distance between the two cursors.

All experiments reported in this paper are performed at aspiration pressures corresponding to uniform, isotropic, membrane tensions (at zero velocity) between 0.12 and 0.38 dyn/cm. A smaller tension results in a nonspherical cell whereas a larger tension usually causes the tether to detach from the bead. (The detachment of a long tether, ~50 μm, results in a dramatic and rapid extension of the membrane tongue into the pipette). Even at fairly low tensions tether detachment often occurred and ended that particular experiment. In experiments where fixed cells are used instead of latex beads, 3% (by wt) of 150,000 mol wt Dextran (Pharmacia Fine Chemicals, Piscataway, NJ) was added to promote adhesion. All experiments were performed at a room temperature of ~23°C.

RESULTS

Measurement of Tether Radius

The principle of conservation of mass permits the tether radius R_t to be expressed in terms of known quantities (Hochmuth and Evans, 1982):

$$R_t = \left(1 - \frac{R_p}{R_c}\right) R_p \left(-\frac{dL_p}{dL_t}\right), \quad (1)$$

where R_p is the radius of the pipette, R_c is the maximum radius of the cell, $-dL_p$ is the decrease in the length of the aspirated portion of the membrane within the pipette and dL_t is the increase in tether length (see Fig. 3).

The movement of the membrane "tongue" down the pipette ($-\Delta L_p$) can be measured with a high degree of precision as shown by Evans et al. (1976). This tracking of the tongue gives accuracies on the order of 10% for overall length changes, $-\Delta L_p$, of 1–2 μm. The change in length of

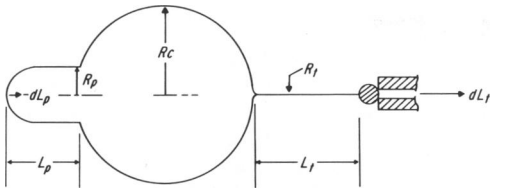

FIGURE 3 Line drawing of a sphered and tethered red cell (compare to Fig. 1). L_p, length of membrane in the pipette, $-dL_p$, change in this length; R_p, radius of the pipette; R_c, radius of the cell; R_t, radius of the tether; L_t, length of the tether; dL_t, change in this length.

the tether, ΔL_t, is measured with the electromechanical linear translator which extracts the tether and provides a digital signal that is proportional to the displacement ΔL_t. Shown in Fig. 4 are plots of L_p vs. L_t. The slopes of these curves are essentially constant and, according to Eq. 1, indicate that the radius remains constant during the tether formation process. The periodicity observed in the data shown in Fig. 4 is caused by a slight nonlinearity in the measurement of L_t. Although the overall slope of the lines shown in Fig. 4 can be measured with an accuracy of ~10%, the calculated value for R_t from Eq. 1 may be no more accurate than ±30% because of an estimated 20% error in the measurement of the pipette diameter caused by optical distortion at the fluid-pipette interface (Fig. 1). With this error in mind, the calculation of a value for R_t follows directly from Eq. 1 and the slope of the L_p vs. L_t line (Fig. 4). A typical calculation for R_t is

$$R_t = [1-(1/3)](1)(1/40) = 0.0166\ \mu m = 166\ \text{Å}$$

when $R_p = 1.0\ \mu m$, $R_c = 3.0\ \mu m$ and $-dL_p/dL_t = 1/40$.

In Fig. 4, a given tether is extracted from a single cell at a fixed isotropic tension ($\bar{T} = 0.19$ dyn/cm) and at four different velocities (0.16, 0.44, 0.84, and 1.63 μm/s). From Eq. 1 and the slopes of the lines shown in Fig. 4, the tether radii are calculated and plotted in Fig. 5. This figure shows that the radius of the tether decreases as the velocity of the tether is increased. Also, the tether radius at zero velocity, R_t^0, is readily obtained from a linear extrapolation. In this particular case $R_t^0 = 176$ Å at $\bar{T} = 0.19$ dyn/cm.

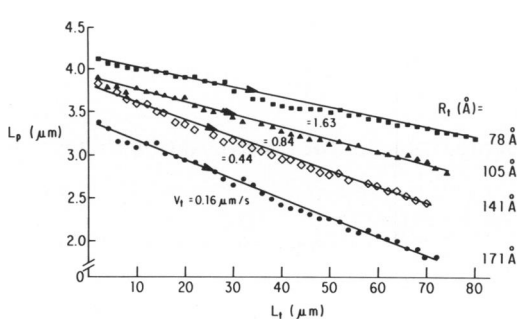

FIGURE 4 Plot of L_p vs. L_t (see Fig. 3) at four different values for the tether velocity, V_t. Shown also are the values for the tether radius, R_t, calculated with Eq. 1. All experiments are performed at a constant isotropic tension in the membrane of $\bar{T} = 0.188$ dyn/cm.

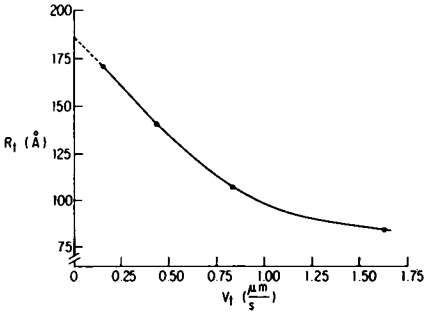

FIGURE 5 Plot of the tether radius as a function of the tether velocity obtained from the results shown in Fig. 4. The dashed line shows a linear extrapolation: $R_t \rightarrow R_t^0$ as $V_t \rightarrow 0$.

Measurement of Membrane Viscosity and Tether Elasticity

The result in Fig. 5 shows clearly that the radius of the tether decreases as the velocity of the tether is increased. As we have shown (Hochmuth and Evans, 1982), this phenomenon is caused by the creation of a tension difference between the axial tension in the tether, $f/2\pi R_t$, and the isotropic tension in the far field, $\bar{T}$:[1]

$$\frac{f}{2\pi R_t} - \bar{T} = \frac{2\eta}{C}\frac{V_t}{R_t}, \qquad (2)$$

where f is the force on the tether, V_t is the velocity of the tether, η is the viscosity of the membrane material as it flows from cell body to tether and C is a correction factor ($C \sim 1.6$) which accounts for the curvature of the membrane material as it flows onto the tether.

The solution of Eq. 2 for R_t reveals that R_t depends on both the force which acts to form the tether and the velocity at which the tether is formed (Hochmuth and Evans, 1982):

$$R_t = \frac{f}{2\pi\bar{T}} - \frac{2\eta V_t}{C\bar{T}}. \qquad (3a)$$

Eq. 3a explains the results shown in Fig. 5. Thus, as the velocity of the tether increases at constant $\bar{T}$, the second term on the right-hand side of Eq. 3a increases at a faster rate than the first term; and, thus, the tether radius decreases.

The observation that the tether radius decreases with increasing velocity allows an interesting prediction to be made with Eq. 3a. That is, for a negative tether velocity (i.e., the tether is being reabsorbed by the cell and V_t is in the negative z direction), the tether radius will increase when the magnitude of the tether velocity increases in the

[1]Since the local membrane tension decreases in direct proportion to the square of the distance from the tether, an isotropic state of tension in the cell membrane is reached within a very short distance from the point where the erythrocyte membrane flows onto the tether.

negative z direction. Mathematically,

$$R_t = \frac{f}{2\pi\bar{T}} + \frac{2\eta|V_t|}{C\bar{T}}, \quad V_t \leq 0. \tag{3b}$$

Eq. 3b predicts that the tether radius will be larger when the tether is reabsorbed ($V_t < 0$). Fig. 6 shows a tether formation and reabsorption experiment performed at constant $\bar{T}$ and $|V_t|$ ($\bar{T}$ = 0.31 dyn/cm and $V_t = \pm 0.27$ μm/s). At the end of the tether formation process (upper line, note the direction of the arrows), the linear translator is stopped for ~20 s and then returned to the cell at the same absolute velocity. During this reabsorption process, there is a period (shown as a dashed line between 70 and 30 μm) during which the tether radius increases steadily until it reaches a new equilibrium value (shown as the solid line with open circles between 30 and 0 μm). During the formation process (0–70 μm), R_t = 113 Å while during the steady-state part of the reabsorption process, R_t = 151 Å.

During the unsteady part of the reabsorption process that occurs between 70 and 30 μm in Fig. 6 the tether radius is increasing with time. In all experiments summarized in Fig. 7, we observe the occurrence of this unsteady component which occurs over a time period of 94 ± 26 s. This non-instantaneous response is caused by dissipation within the tether, possibly because of either bulk flow of liquid (e.g., concentrated hemoglobin solution) into the tether or relative slip and dissipation of the multilamellar structure (i.e., lipid bilayer plus, possibly, a proteinaceous layer) that forms the tether membrane.

The results of a series of these out and back experiments are shown in Fig. 7. A two-point interpolation between the out (smaller radius) and back (larger radius) experiments permit a determination of the tether radius at zero velocity, R_t^0. In several instances, two- and three-point extrapolations of data like that shown in Fig. 5 are used to obtain a value for R_t^0. In general, the intercept values for R_t (R_t = R_t^0 at V_t = 0) shown in Fig. 7 are >150 Å when the isotropic tension is relatively small ($\bar{T}$ = 0.13–0.19 dyn/cm) while the values for R_t^0 are <150 Å when the isotropic tension is relatively large ($\bar{T}$ = 0.31–0.38 dyn/cm). A plot of the values for R_t^0 and $\bar{T}$ (Fig. 8) demonstrates the elastic behavior of the tether.

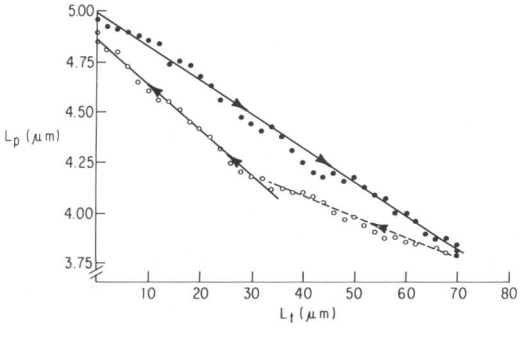

FIGURE 6 Results from an out and back experiment. The upper solid line (●) shows the extraction of the tether at a constant velocity, V_t = 0.27 μm/s. The lower solid line (○) shows the reabsorption of the tether at an equal and opposite velocity, V_t = −0.27 μm/s. The dashed line represents an unsteady-state situation in which the tether radius is steadily increasing in size from its original value in the out experiment to a larger value in the back experiment. $\bar{T}$ = 0.31 dyn/cm.

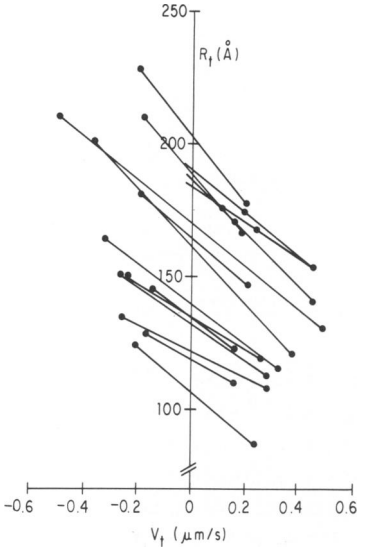

FIGURE 7 Plot of thirteen out and back experiments such as those shown in Fig. 6 and two extraction experiments such as those shown in Figs. 4 and 5. In all cases, the tether radius at zero velocity, R_t^0, is determined either by interpolation or extrapolation. In general, the larger radii (R_t^0 > 150 Å) are for smaller isotropic tensions (0.13 dyn/cm ≤ $\bar{T}$ ≤ 0.20 dyn/cm) while the smaller radii (R_t^0 < 150 Å) are for larger isotropic tensions (0.30 dyn/cm ≤ $\bar{T}$ ≤ 0.38 dyn/cm).

Eq. 3 and the data shown in Figs. 7 and 8 permit a calculation for the membrane viscosity η. As we have shown (Hochmuth and Evans, 1982), the derivative of Eq. 3 with respect to V_t, along with a substitution for the tether force f, $f^0 = 2\pi R_t^0 \cdot \bar{T}$, leads to the following expression for the viscosity:

$$\eta = \frac{C}{2} R_t^0 \left(\frac{dT}{dR_t^0}\right)\left(\frac{\partial R_t}{\partial V_t}\right)_{\bar{T}}. \tag{4}$$

Fig. 8 shows that

$$\frac{d\bar{T}}{dR_t^0} = -2.88 \times 10^5 \text{ dyn/cm}^2$$

The average value for the slopes of the lines shown in Fig. 7 is

$$\frac{\partial R_t}{\partial V_t} = -0.0080 \pm 0.0021 \text{ s}^{-1}.$$

The average value for the tether radius at zero velocity, R_t^0, as shown in Fig. 8, is

$$R_t^0 = 151 \text{ Å}.$$

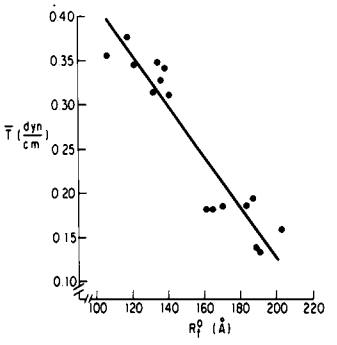

FIGURE 8 Plot of the tether radius at zero velocity ($R_t = R_t^0$ at $V_t = 0$; Fig. 7) as a function of the isotropic tension in the membrane.

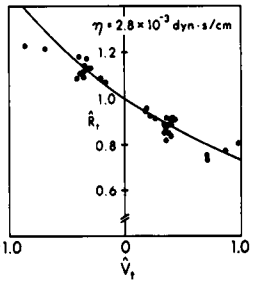

FIGURE 9 Plot of the data of Fig. 7 in terms of the dimensionless tether radius and velocity: $\hat{R}_t = R_t/R_t^0$, $\hat{V}_t = 2\eta V_t/R_t^0\bar{T}$. The solid curve is from the analytical solution of Hochmuth and Evans (1982; Fig. 7) for the particular case $\hat{f} = 1/\hat{R}_t$.

Thus, with these values and Eq. 4, we can calculate a typical value for the membrane surface viscosity:

$$\eta = 2.8 \times 10^{-3} \frac{\text{dyn} \cdot \text{s}}{\text{cm}}.$$

With this particular value for the surface viscosity, the results shown in Fig. 7 should collapse onto a single curve when scaled according to the analysis in the previous paper (Hochmuth and Evans, 1982). Thus, all data in Fig. 7 are plotted in Fig. 9 with $\hat{R}_t = R_t/R_t^0$, $\hat{V}_t = 2\eta V_t/R_t^0\bar{T}$ and $\eta = 2.8 \times 10^{-3}$ dyn·s/cm. The solid curve shown in Fig. 9 is from our analytical solution of the tether flow problem (Hochmuth and Evans, 1982; Fig. 7) when the elastic behavior of the tether is given by $\hat{f} = 1/\hat{R}_t$.

DISCUSSION

Since the isotropic tension in the cell membrane is equal to the axial tension acting on the tether when $V_t = 0$, Fig. 8 shows an inverse relation between the axial tension and the tether radius. With this result, it is easy to show that the axial force f also varies inversely with R_t^0:

$$f^0 = 2\pi R_t^0 \bar{T}$$

$$\frac{df^0}{dR_t^0} = 2\pi R_t^0 \frac{d\bar{T}}{dR_t^0} + 2\pi\bar{T} = -1.32 \frac{\text{dyn}}{\text{cm}}$$

for $R_t^0 = 160$ Å and $\bar{T} = 0.25$ dyn/cm. (These values for R_t^0 and $\bar{T}$ are chosen at the mid-point of the straight line drawn in Fig. 8). Intuitively, this result is correct, since we would expect the tether radius to decrease as the force on the tether is increased.

The flow-channel studies of Hochmuth et al. (1973) indicate that the tether can undergo an elastic response and that the length of the tether increases linearly with force relative to some zero-force reference length L_o (and zero force tether radius R_o). In those experiments, the tether is extended rapidly by imposing a constant fluid shear force on the erythrocyte. (Following this rapid elastic response, membrane material flows steadily from cell body to tether and, thus, the tether slowly increases in length.) This rapid elastic extension occurs essentially at constant membrane surface area:

$$R_oL_o = R_t^0L_t^0 \tag{5}$$

where R_t^0 and L_t^0 represent the tether radius and length in an extended state. When the original results of Hochmuth et al. (Fig. 5; 1973) are expressed in terms of the force acting on the cells (which is calculated by mutliplying the fluid shear stress by an estimated cell surface-area of 50 μm^2) and when the constant surface-area relation is employed (Eq. 5), the following result is obtained:

$$f^0 = K_t(R_o/R_t^0 - 1) \tag{6}$$

where $K_t = 0.66 \times 10^{-6}$ dyn and $R_o = 0.1$ μm (an estimate). Note that since $R_o/R_t^0 >> 1$, it is reasonable to assume a simple inverse relation between the tether force and tether radius: $f \sim 1/R_t$. The derivative of Eq. 6 can be applied (extrapolated) to the region represented by the data in Fig. 8:

$$\frac{df^0}{dR_t^0} = -\frac{K_tR_o}{(R_t^0)^2} = -2.57 \frac{\text{dyn}}{\text{cm}}$$

for $R_t^0 = 160$ Å. This result is in reasonable agreement with the results obtained directly from the data shown in Fig. 8 ($df^0/dR_t^0 = -1.32$ dyn/cm) and, thus, we are confident that the result shown in Fig. 8 is a reasonable representation of the elastic behavior of the tether for the range of values shown in the figure.

Several mechanisms can be suggested to account for the elastic behavior of the tether. Among these are: (*a*) an elastic shear rigidity associated with the tether membrane, (*b*) a bending rigidity associated with the membrane and, (*c*) a spongy proteinaceous mass (e.g., spectrin, concentrated hemoglobin, etc.) contained within the tether. An analysis of (*c*) is beyond the scope of this paper. However, an order-of-magnitude analysis given below of (*a*) and (*b*) indicates that either or both could account for the elastic behavior of the tether.

If we model the tether as a very thin cylindrical shell, then the axial force would be related to the shear modulus by the following expression:[2]

$$\frac{f^0}{2\pi R_t^0} \approx \mu \lambda^2 = \mu \left\{\frac{R_o}{R_t^0}\right\}^2$$

or

$$f^0 = \frac{2\pi\mu R_o^2}{R_t^0} \tag{7}$$

where μ is the elastic shear modulus and R_o is defined in Eq. 5. The derivative of Eq. 7 and its subsequent evaluation for reasonable values of R_o and R_t^0 of 0.1 μm and 160 Å give

$$\frac{df^0}{dR_t^0} = -\frac{2\pi\mu R_o^2}{(R_t^0)^2} = -1.47\,\frac{\text{dyn}}{\text{cm}}$$

when $\mu = 0.006$ dyn/cm. This value agrees closely with the measured value of -1.32 dyn/cm.

The bending energy (Evans and Hochmuth, 1978) in a tether of length L_t^0 and radius R_t^0 would be on the order of

$$\frac{B}{2(R_t^0)^2}(\pi R_t^0 L_t^0)$$

where B is the curvature elastic energy. If the tether is modeled as a coupled bilayer, we estimate a value for B of 3×10^{-12} dyn·cm (Evans and Hochmuth, 1978). If the bilayers are uncoupled (i.e., relative slip occurs between the two halves of the bilayer), then the value for B would be at least an order of magnitude smaller. A virtual increase in tether length, δL_t^0, produced by the tether force f^0 results in an increase in the stored elastic energy of the tether. If we assume that this energy increase is due to bending, then

$$f^0 \cdot \delta L_t^0 = \frac{\pi B}{2R_t^0}\delta L_t^0$$

or

$$f^0 = \frac{\pi B}{2R_t^0}. \tag{8}$$

The derivative of Eq. 8 gives

$$\frac{df^0}{dR_t^0} = -\frac{\pi B}{2(R_t^0)^2} = -1.84\,\frac{\text{dyn}}{\text{cm}}$$

when $R_t^0 = 160$ Å and $B = 3 \times 10^{-12}$ dyn·cm. Again we note that this value agrees closely with the measured value of -1.32 dyn/cm.

[2]The circumferential tension can be neglected relative to the axial tension since their ratio is on the order of the tether radius divided by the pipette radius.

In the analysis of the present experiments (Hochmuth and Evans, 1982), we assume that the cell membrane flows as a Newtonian fluid and, thus, the viscosity of the membrane is constant regardless of its rate of deformation. As membrane material flows from cell body to tether, the rate of deformation of a material element increases from zero to a maximum value (which is on the order of the ratio of the tether velocity to the tether radius: V_t/R_t) and then returns to zero as the membrane material element reaches the tether. The characteristic rate of deformation (V_t/R_t) is increased by increasing the velocity of the tether (Fig. 5). For example, the four data points shown in Fig. 5 give values for V_t/R_t of 9.4, 32, 78, and 200 s^{-1}. The first three data points appear to fall on a straight line and, thus, indicate that the viscosity remains constant as long as the elastic behavior ($d\bar{T}/dR_t$; Fig. 8) remains constant in this region (107 Å $\leq R_t^0 \leq$ 171 Å). However, the final point (R_t = 83 Å) indicates a decrease in the slope of the R_t vs. V_t line. At this point the tether radius is probably approaching a geometric limit caused by the finite thickness of the erythrocyte membrane. In addition, recent data (not shown) indicate that the slope of the $\bar{T}$ vs. R_t^0 line shown in Fig. 8 becomes steeper when the tether radius is <100 Å. Therefore, although ($\partial R_t/\partial V_t$) decreases when $R_t < 100$ Å (Fig. 5), $d\bar{T}/dR_t^0$ appears to increase in this region with a net result that the viscosity of the tether, as calculated from the product of these two slopes (Eq. 4), may remain constant. However, it should be noted that the tether radius also appears as a product in Eq. 4. Thus, not only must the two changing slopes compensate for each other, they must also compensate for the change in tether radius with changing tension in order for η to remain constant in this region. The worst case analysis in which we assume that $d\bar{T}/dR_t^0$ remains constant throughout the entire range of the experiment indicates, at most, that the viscosity of the membrane material decreases by a factor of 2 when the characteristic rate of deformation (V_t/R_t) is increased from 10 to 200 s^{-1}. Thus, in these experiments we see little evidence for a significant shear thinning of the membrane viscosity at high rates of deformation.

In their studies of the flow of membrane material from a flaccid cell to a tether, Evans and Hochmuth (1976*b*) and Hochmuth et al. (1976) obtain a value for the membrane viscosity which is on the order of 10^{-2} SP (1 SP = 1 poise·cm = 1 dyn·s/cm). This value is in reasonable agreement with the present measurement ($\eta = 3 \times 10^{-3}$ SP) especially since the original tether flow experiments involve a non-axisymmetric configuration in which a cylindrical tether is extracted from the rim of a disklike erythrocyte. In addition, in those experiments the actual force on the cell is estimated from the product of the measured value for the fluid shear stress and an approximate value for the membrane surface area.

Other measurements for membrane surface viscosity involve the relatively slow and gentle recovery of the erythrocyte membrane after it has been deformed with a

pipette (Evans and Hochmuth, 1976*a*; Hochmuth et al., 1979; Chien et al., 1978). These measurements give a value for the membrane viscosity that is $\sim 6\text{–}8 \times 10^{-4}$ SP. This value is about a factor of 4 or 5 less than the present measurements. We can only speculate that a drastic deformation and rearrangement of the structural material in the membrane produces a relatively large resistance to flow compared with the resistance encountered in the erythrocyte recovery experiments.

Recently, Waugh (1982) has measured the rate of formation of tethers extracted from spherical lipid vesicles when the vesicles are subjected to a fluid shear force. From these studies Waugh estimates a maximum value for the lipid viscosity of $\sim 10^{-5}$ SP, which is at least two orders of magnitude less than the value we have measured for erythrocyte membranes. Certainly the complex protein-lipid structure of the erythrocyte membrane accounts for the much larger value for the viscosity.

Since the tether radius is calculated from a mass balance (Hochmuth and Evans, 1982), it is a mean-mass radius. That is, the value for R_t represents the distance from the center of the tether to a circumferential line which divides the mass of the membrane into two equal parts. If the planar membrane has an effective thickness of, say, 100 Å and if the density of the membrane is constant, then the absolute minimum value for R_t would be 71 Å. The minimum values for R_t in these experiments are between 70 and 80 Å (Figs. 5 and 7).

In our analysis of the tether flow problem (Hochmuth and Evans, 1982), we tacitly assume that the membrane thickness is much smaller than the tether radius. However, we are approaching an opposite situation in which the radius and thickness are similar in magnitude (Figs. 5, 7, 8). In addition, a small tether radius will force the two lipid monolayers and, possibly, the inner protein layer to slip relative to each other. (The inner layer or layers will extrude into the body of the cell and become compressed relative to the outer surface layer.) Therefore, future analyses of axisymmetric membrane flow must deal with the problem of finite membrane thickness and slip; and future experiments must be designed to determine if all of the cellular membrane is capable of flowing from cell body to tether.

This work was supported by National Institutes of Health grant HL 23728.

Received for publication 16 June 1981 and in revised form 19 January 1982.

REFERENCES

Chien, S., K.-L. P. Sung, R. Skalak, S. Usami, and A. Tozeren. 1978. Theoretical and experimental studies on viscoelastic properties of erythrocyte membrane. *Biophys. J.* 24:463–487.

Evans, E. A., R. Waugh, and L. Melnik. 1976. Elastic area compressibility modulus of red cell membrane. *Biophys. J.* 16:585–595.

Evans, E. A., and R. M. Hochmuth. 1976 a. Membrane viscoelasticity. *Biophys. J.* 16:1–11.

Evans, E. A., and R. M. Hochmuth. 1976 b. Membrane viscoplastic flow. *Biophys. J.* 16:13–26.

Evans, E. A., and R. M. Hochmuth. 1978. Mechano-chemical properties of membranes. *Curr. Top. Membr. Transp.* 10:1–64.

Hochmuth, R. M., N. Mohandas, and P. L. Blackshear, Jr. 1973. Measurement of the elastic modulus for red cell membrane using a fluid mechanical technique. *Biophys. J.* 13:747–762.

Hochmuth, R. M., E. A. Evans, and D. F. Colvard. 1976. Viscosity of human red cell membrane in plastic flow. *Microvascular Res.* 11:155–159.

Hochmuth, R. M., P. R. Worthy, and E. A. Evans. 1979. Red cell extensional recovery and the determination of membrane viscosity. *Biophys. J.* 26:101–114.

Hochmuth, R. M., and E. A. Evans. 1982. Extensional flow of erythrocyte membrane from cell body to elastic tether: I. Analysis. *Biophys. J.* 39:71–81.

Waugh, R. E. 1982. Surface viscosity measurements from large bilayer vesicle tether formation. I. Analysis. *Biophys. J.* 38:15–18.

Waugh, R. E. 1982. Surface viscosity measurements from large bilayer vesicle tether formation. II. Experiments. *Biophys. J.* 38:19–28.